2018 EAGE ANNUAL
80TH CONFERENCE + EXHIBITION
COPENHAGEN | DENMARK

Th A12 09

Migration Confidence Analysis: Resolved Space Uncertainties

J. Messud* (CGG), P. Guillaume (CGG), M. Reinier (CGG), C. Hidalgo (INEOS)

Summary

We show how the method recently proposed in Messud et al. (2017; 2017b) allows consideration of “resolved space” tomographic uncertainties which are complementary information to the total tomographic uncertainties. Resolved space uncertainties are obtained by restricting the tomography model space to the one that can be resolved by tomography. Total uncertainties mostly quantify the illumination uncertainties, whereas resolved space uncertainties tend to be more correlated to the final tomography model. We illustrate how those two uncertainties give complementary information for the subsequent seismic interpretation.

Introduction

Seismic imaging deliveries are a basis for seismic interpretation and downstream E&P activities. The accuracy of the positioning of imaged seismic reflectors greatly depends on the migration "velocity" model ("velocity" here stands for all anisotropy parameters), since it directly affects lateral and vertical positioning and thus the shape of migrated structures. Several publications have addressed the estimation of structural uncertainties within the frame of ray-based tomography (Duffet and Sinoquet, 2006; Osypov et al., 2013), the most widely used tool in the industry for velocity model building. They typically involve two main steps after final tomography: first the generation of a set of consistent perturbed velocities by exploration of the *a posteriori* probability density function (PDF) within the Gaussian approximation; second, computation of statistical uncertainty attributes (such as depth standard deviations) for key horizons after migrations in perturbed models.

Likewise, Messud et al. (2017) recently proposed an original approach where the exploration of the *a posteriori* PDF is performed along the equi-probable contour related to the standard deviation confidence level, thus optimizing the exploration of the PDF without any information loss under the Gaussian approximation. Unlike previous approaches (Osypov et al., 2013), this one is applied in a non-linear tomography context with the advantage of providing a QC of the validity of the Gaussian approximation. This has been described by Messud et al. (2017b) and illustrated by Messud et al. (2017) and Reinier et al. (2017).

Here, we develop further our approach by limiting computation of uncertainties to the "resolved space". Tomography problems mix two sources of information: input data (picks) and regularizations. In "total space" uncertainties, regularizations and illumination contributions dominate over the input data contribution. As a consequence, total uncertainties largely tend to quantify the uncertainties related to regularizations and illumination (Messud et al., 2017). In this situation, minimal model space restriction is considered in the computation of the perturbations. Complementary information could be obtained by computing uncertainties which are constrained more by the input data than by the regularizations. This can be achieved by restricting the computation of the perturbations to the model space that can be resolved by tomography, i.e. the space constrained only by input data. As it leads to velocity perturbations that are more structurally consistent, the resolved space uncertainties tend to be more correlated to the final tomography velocity. The use of this complementary information is illustrated below.

Compute perturbations in resolved space

Uncertainties relating to velocity model parameters can be evaluated by developing a PDF around the model obtained by final tomography, which is assumed to be the maximum likelihood model. This model is denoted by a vector $\boldsymbol{m}_0$ of dimension N (in practice N ranges from 500,000 to 50 million parameters). A method proposed by Messud et al. (2017b) assumes that the PDF has a Gaussian distribution in a sufficiently large interval. It computes equi-probable velocity model perturbations that bound the standard deviation-like (or 68.3%) confidence level, defined by

$$\Delta \boldsymbol{m} = \alpha\, \boldsymbol{B}\, \boldsymbol{\delta r} \quad , \quad \boldsymbol{\delta r}^{+} \boldsymbol{\delta r} = 1 \quad , \qquad (1)$$

where α is a scalar computed from the quantile of order 68.3% of the Chi-squared distribution, "$^+$" denotes the matrix transpose and $\boldsymbol{\delta r}$ is a unit random vector of dimension N allowing to generate the perturbations. $\boldsymbol{B}$ is a "square root" of the inverse of the tomography Hessian $N \times N$ matrix built from the linearized tomographic forward operator, data quality factors and the tomography regularizations (amongst other a Tikhonov regularization expressed as $\varepsilon \boldsymbol{I}_N$, ε being a damping level fixed a priori). We approximate $\boldsymbol{B}$ by an eigenvalue decomposition of the Hessian (EVD) (Zhang and McMechan, 1995) which is restricted to eigenvalues greater than ε. p is the corresponding number of eigenvectors. The effect of the non-computed $N - p$ eigenvectors is approximated by $\varepsilon \boldsymbol{I}_N$. After manipulations using the binomial inverse theorem (Osypov et al, 2013; Messud et al, 2017), we obtain

$$\boldsymbol{B} = \boldsymbol{B}^{resolved} + \boldsymbol{B}^{un-resolved} \qquad (2)$$
$$\boldsymbol{B}^{resolved} = \boldsymbol{D}\boldsymbol{V}_p \left(\Delta_p + \varepsilon \boldsymbol{I}_p\right)^{-1/2} \boldsymbol{V}_p^{+} \quad , \quad \boldsymbol{B}^{un-resolved} = \boldsymbol{D}(\boldsymbol{I}_N - \boldsymbol{V}_p \boldsymbol{V}_p^{+})\varepsilon^{-1/2}$$

$\boldsymbol{V}_p$ and Δ_p contain the p eigenvectors and eigenvalues. Because an EVD cannot mix different physical quantities, we introduced the diagonal and invertible matrix $\boldsymbol{D}$ to simply rescale, within the EVD, the various physical units in the model space and possibly compensate for subsurface illumination.

From eq. (2) we see that two contributions appear in $\boldsymbol{B}$:

- $\boldsymbol{B}^{resolved}$ drives the contribution in $\Delta\boldsymbol{m}$ of the eigenvectors with eigenvalues above the priori damping level ε, which span the so-called tomography resolved space. As those eigenvectors are greatly constrained by the tomography input data, so are the related perturbations $\Delta\boldsymbol{m}^{resolved} = \alpha\, \boldsymbol{B}^{resolved}\, \boldsymbol{\delta r}$. They tend to be more structurally consistent and smooth (because tomography resolves the large wavelengths of the velocity model), as illustrated in Fig. 1c.
- $\boldsymbol{B}^{un-resolved}$ drives the contribution in the uncertainties of eigenvectors eigenvalues below ε, which span the tomography "unresolved space". This space represents the effective null space of full tomography, constrained only by the regularizations and not by the input data. The related perturbations $\Delta\boldsymbol{m}^{un-resolved} = \alpha\, \boldsymbol{B}^{un-resolved}\, \boldsymbol{\delta r}$ are less structurally consistent, but are not without interest. They give information focused on what tomography cannot resolve, mainly related to illumination issues, which is a major source of uncertainties.

Total perturbations as shown in eq. (1), are given by the sum of both contributions. An example is given in Fig. 1b.

Computing uncertainty attributes

Uncertainty attributes can be computed statistically using the obtained set of perturbations for both total space, using the $\{\Delta\boldsymbol{m}\}$, and resolved space, using the $\{\Delta\boldsymbol{m}^{resolved}\}$. For example:

- Tomography velocity error bars: Error bars on $\boldsymbol{m}_0$ (for instance on V_p and ε models) can be computed by considering the maximum possible variations of the model perturbations. Reinier et al. (2017) give an illustration for the total space.
- Horizon error bars: Map (or zero-offset kinematic) migrations can be performed in each perturbation to obtain a set of horizon perturbations that can be proven to be equi-probable and to bound the standard deviation-like confidence region (Messud et al., 2017b). A depth error bar can be defined as the maximum possible depth variation of the horizon perturbations (Messud et al., 2017b). Lateral (x and y-directions) error bars can be computed using the same principle, from differences of position between rays traced in $\boldsymbol{m}_0$ and rays traced in the perturbed model.

Originality of our method

In their method, Osypov et al (2013) use an equation similar to eq. (2). A key difference from our method is that their matrix $\boldsymbol{D}$ is related to the tomography regularizations they use, amongst other steering filters (that are non-invertible, with their own null space). As a consequence, their perturbations are always projected on their tomography regularizations, leading to structurally consistent perturbations. Nothing can be explored in the null space of the steering filters.

In our method $\boldsymbol{D}$ has no relation to tomography regularizations and is fully invertible. As a consequence, we can compute total uncertainties that account for the null space of the full tomography (or unresolved space). This is significant because the major contribution to uncertainties comes from what tomography cannot resolve, which can be quantified by the total uncertainties. We can also restrict the model space to structurally more consistent perturbations and compute the resolved space uncertainties. We now illustrate how those uncertainties give complementary information.

3D field data example

The real data example is typical of the North Sea area with the usual challenges (shallow channels, strong vertical velocity contrasts, etc.). The method was tested in the context of a depth velocity model building for INEOS. The data, acquired with conventional marine acquisition, is used to illustrate the horizon uncertainties in both resolved and total spaces. A TTI model with 5 layers was updated iteratively using both full waveform inversion up to 13 Hz and ray-based tomography. 200 model perturbations were computed in each layer simultaneously for V_p and ε parameters.

Fig 1 shows the V_p model component of one perturbation in the resolved space $\Delta \boldsymbol{m}^{resolved}$ versus the total perturbation $\Delta \boldsymbol{m} = \Delta \boldsymbol{m}^{resolved} + \Delta \boldsymbol{m}^{un-resolved}$. The resolved space perturbation looks more organized than the total perturbation, smoother, and more correlated to structures and the tomography final model. The total perturbation with the same parametrization looks more random and higher frequency, mainly because the tomography unresolved space is large and thus a dominant contributor to the total perturbation (i.e. the magnitude of $\Delta \boldsymbol{m}^{un-resolved}$ is larger, here approximately 4 times, than the magnitude of $\Delta \boldsymbol{m}^{resolved}$).

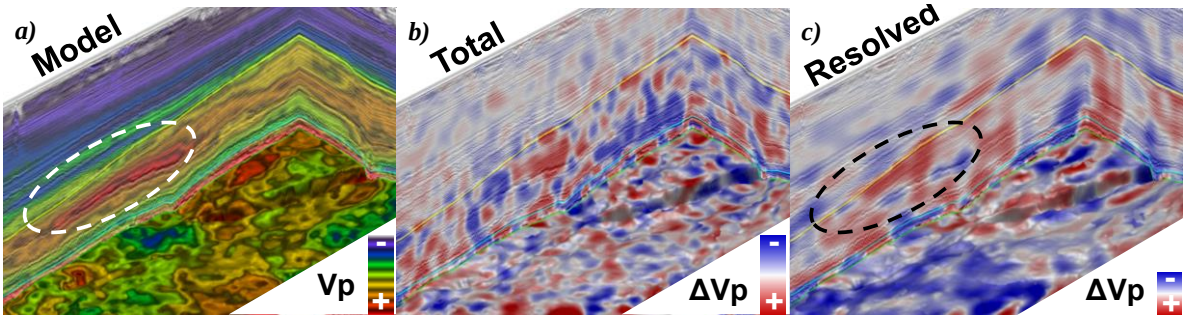

Figure 1 *V_p model (Left) and perturbations, displayed on sections and extracted on the Top Chalk horizon. Middle: Total space. Right: Resolved space.*

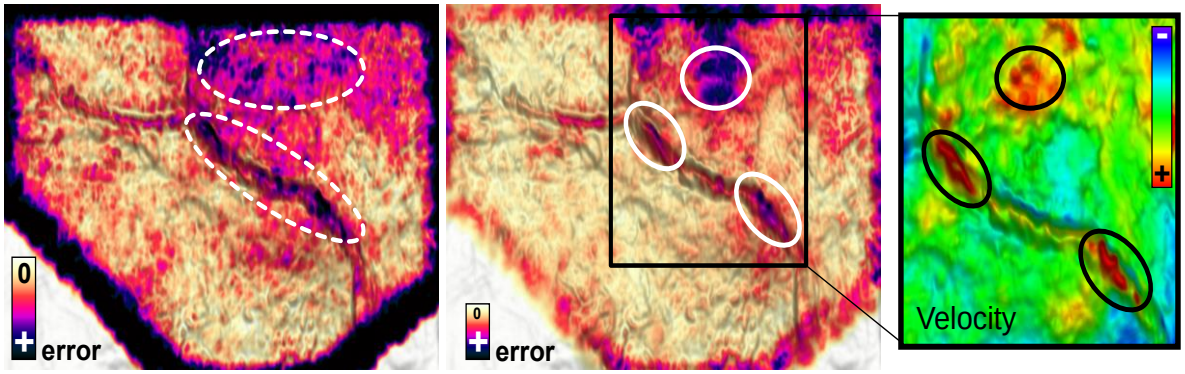

Figure 2 *Error bars in depth z-direction. Left: Total space. Middle: Resolved space. Right: V_p extracted above the horizon.*

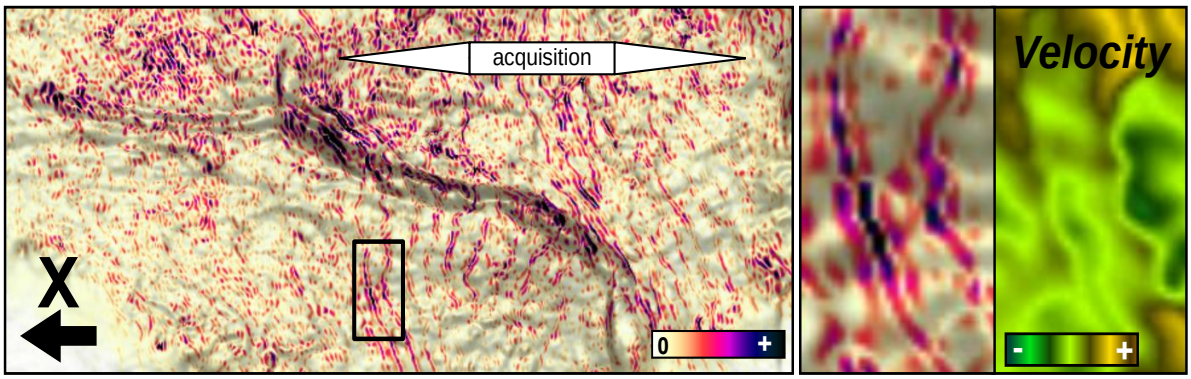

Figure 3 *Error bars in x-direction for the resolved subspace of Top Chalk horizon (Left). Zoom of error bar and of V_p depth slice above the horizon (Right).*

The Top Chalk key horizon was map migrated into the 200 generated perturbed models and associated error bars computed. Fig. 2 shows depth error bars width, in total and resolved spaces. The total depth error bars are dominated by the acquisition illumination variations, less illumination resulting in higher uncertainties. The narrow canyon in the middle of the map is incompletely illuminated and therefore appears with larger error bars. Resolved space depth error bars appear to be correlated to high frequency velocity variations: local significant vertical or lateral velocity variations tend to produce higher uncertainties. For instance, the localized higher V_p in the layer above Top Chalk generates higher uncertainties in resolved space (see surrounded areas in Fig. 2). Those error bars are also correlated with the reliability and richness of the picks (mainly characterized by angle diversity) that feed the tomography (Messud et al., 2017).

Lateral (x-direction) horizon error bars in resolved space are shown in Fig. 3. Again, their hierarchies tend to be correlated with velocity variations: subtle lateral velocity variations (due to faults aligned along the y-direction) perpendicular to the x-direction tend to generate higher lateral horizon error bars. Thus in this case the x-direction error bars tend to underline the faults. Higher velocity variations produce higher uncertainties.

Both total and resolved space uncertainties provide detailed information on the subsurface, but from different points of view. Total uncertainties quantify the illumination uncertainties and resolved space uncertainties highlight more the local velocity variation effects.

Conclusions

We have presented a method providing uncertainties in the tomography resolved space in complement to total uncertainties. Resolved space uncertainties tend to be more correlated to the final tomography model (as they are obtained from perturbations that follow the structures). Total uncertainties mostly quantify the illumination uncertainties.

Acknowledgements

We thank WesternGeco, INEOS and CGG for their permission to publish this work. We gratefully thank Gilles Lambaré, Vincent Prieux and Hervé Prigent for their support.

References

Duffet, C. and Sinoquet, D. [2006] Quantifying uncertainties on the solution model of seismic tomography. *Inverse Problems*, **22**, 525-538.

Guillaume, P., Zhang, X., Prescott, A., Lambaré, G., Reinier, M, Montel, J-P and Cavalié, A. [2013] Multi-layer non-linear slope tomography. *75th EAGE Conference & Exhibition*, Extended Abstracts, Th 04 01.

Messud, J., Reinier, M., Prigent, H., Guillaume, P., Coléou, T. and Masclet, S. [2017] Extracting seismic uncertainties from tomographic velocity inversion and their use in reservoir risk analysis. *The Leading Edge*, February 2017.

Messud, J., Guillaume, P. and Lambaré, G. [2017b] Estimating structural uncertainties in seismic images using qui-probable tomographic models. *79th EAGE Conference & Exhibition*.

Osypov, K., Yang, Y., Fourier, A., Ivanova, N., Bachrach, R., Yarman, C. E., You, Y., Nichols, D. and Woodward, M. [2013] Model-uncertainty quantification in seismic tomography: method and applications. *Geophysical Prospecting*, **61**, 1114-1134.

Reinier, M., Messud, J., Guillaume, P. and Rebert, T. [2017] Estimating structural uncertainties in seismic images using qui-probable tomographic models. *79th EAGE Conference & Exhibition, Workshop*.

Zhang, J. and McMechan, G. A. [1995] Estimation of resolution and covariance for large matrix inversions. *Geophysical Journal International*, **121**, 409-426.